Applied Catalysis B: Environmental 91 (2009) 355–361

Contents lists available at ScienceDirect

Applied Catalysis B: Environmental

journal homepage: www.elsevier.com/locate/apcatb

Carbon-doped TiO_2 photocatalyst synthesized without using an external carbon precursor and the visible light activity

Yiseul Park [a], Wooyul Kim [a], Hyunwoong Park [b], Takashi Tachikawa [c], Tetsuro Majima [c], Wonyong Choi [a,*]

[a] School of Environmental Science and Engineering, Pohang University of Science and Technology (POSTECH), Hyoja-dong, Pohang 790-784, Republic of Korea
[b] School of Physics and Energy Science, Kyungpook National University, Daegu 702-701, Republic of Korea
[c] The Institute of Scientific and Industrial Research (SANKEN), Osaka University, Osaka 567-0047, Japan

ARTICLE INFO

Article history:
Received 18 April 2009
Received in revised form 1 June 2009
Accepted 4 June 2009
Available online 10 June 2009

Keywords:
TiO_2
Carbon dopant
Visible light photocatalyst
Sol–gel synthesis
Photooxidation

ABSTRACT

Carbon-doped TiO_2 (C-TiO_2) was successfully prepared from a conventional sol–gel synthesis without using external carbon precursors whereas all the previous reports on the synthesis of C-TiO_2 utilized them. The carbons contained in titanium alkoxide precursor could be incorporated into the lattice of TiO_2 with creating mid-bandgap electronic states through the controlled calcination. The level of carbon doping was changed sensitively depending on the calcination temperature, which was verified by UV–visible diffuse reflectance spectroscopy and X-ray photoelectron spectroscopy. The charge pair generation/recombination in C-TiO_2 was compared under visible and UV light through a time-resolved diffuse reflectance spectroscopy study, which suggested the presence of midgap energy levels induced by the incorporation of carbon dopants. The carbon doping was maximal when the calcination temperature was around 200–250 °C and hindered at higher temperatures. The visible light activities of the prepared TiO_2 samples for the conversion of 4-chlorophenol and iodide were also strongly dependent on the calcination temperature and maximized at around 250 °C. This study implies that the carbon doping in TiO_2 can be obtained even unintentionally in the conventional sol–gel synthesis.

1. Introduction

Titanium dioxide has been the most popular photocatalyst due to high photo-oxidation power, excellent stability, non-toxicity, and low material cost. The photocatalytic reactions on TiO_2 are initiated by bandgap excitation and the subsequent generation and transfer of electron (e_{cb}^-) and hole (h_{vb}^+) pairs [1]. In general, TiO_2 with a large bandgap (~3.2 eV) is activated only under UV light irradiation, which is a major drawback. Therefore, it has been modified by various ways such as dye sensitization [2,3] and transition metal doping [4–6], enabling the photocatalyst to operate under visible light irradiation. Recently, researchers have reported that doping TiO_2 with non-metals such as N, S or C extends the absorption wavelengths from UV to visible region, which has been ascribed to the introduction of localized electronic states in the bandgap [7–10].

The intentional and controlled incorporation of carbon impurities into TiO_2 lattice is an efficient method to induce visible light photocatalytic activity [11–18]. TiO_2-mounted activated carbon [19,20] and carbon-coated TiO_2 [21,22] have been also investigated for their photocatalytic activity but the role of carbon in these cases is related mainly with enhancing the adsorption of organic substrates. The carbon-doped TiO_2 (C-TiO_2) has been prepared using different synthetic methods and the state of impurity carbons in the TiO_2 lattice has been interpreted differently. In the literature, the carbon dopant has been described either as an anion that replaces oxygen substitutionally in the lattice [11–14] or as a cation that occupies an interstitial lattice site [15–18]. The formal oxidation state of carbon dopants ranges from −4 (as carbides with Ti–C bond) to +4 (as carbonates with C–O bond) [9]. Ti–C bond was formed at conditions like flame pyrolysis of Ti metal sheet, annealing of TiC powders [11–13], and ion-assisted electron beam evaporation. On the other hand, C–O bond (carbonate) was often observed at conditions like sol–gel processes with carbon precursors and high temperature reactions of TiO_2 with carbon precursors [15–18]. The existence of the former or the latter state seems to be strongly dependent on the preparation method and condition. Both carbon states may be even co-present depending on the preparation condition [23]. Although carbon is a ubiquitous impurity, the addition of external carbon precursors (e.g., alkylammonium, urea, glucose) was essentially needed to make C-TiO_2 in all reported cases.

In this study, we note that the common precursors of TiO_2, titanium alkoxides, contain organic carbons which might be incorporated into the oxide lattice as an impurity dopant during synthesis even in the absence of extra carbon precursors.

* Corresponding author. Tel.: +82 54 279 2283; fax: +82 54 279 8299.
E-mail address: wchoi@postech.edu (W. Choi).

0926-3373/$ – see front matter © 2009 Elsevier B.V. All rights reserved.
doi:10.1016/j.apcatb.2009.06.001

We synthesized C-TiO_2 through a sol–gel route (using titanium butoxide as a precursor of both Ti and C) and an incomplete calcination at low temperature. Although the post-heat treatment (calcination) usually removes all carbon residues, a controlled calcination at temperature ranging from 200 to 300 °C could leave some carbon species as a dopant within the TiO_2 lattice. Various experimental characterizations of the material properties and photocatalytic activities confirmed that the TiO_2 prepared in the absence of external carbon precursors was indeed C-TiO_2.

2. Experimental

2.1. Catalyst preparation and characterization

C-TiO_2 was prepared according to a typical sol–gel method. 32 mmol of titanium butoxide ($Ti[O(CH_2)_3CH_3]_4$, Aldrich) was dissolved in 50 ml of 2-propanol, and then $HClO_4$ solution (7 mmol) was added dropwise under vigorous stirring in an ice bath. The resulting gel was aged at room temperature for 1 day and dried in an oven at 80 °C and subsequently heat-treated in a furnace at various temperatures with a ramping rate of 5 °C/min for 3 h.

The phase identification of C-TiO_2 was carried out by powder X-ray diffraction (XRD) using Cu Kα radiation (Mac Science Co. M18XHF). The BET surface area measurements were carried out using nitrogen as an adsorptive gas. Diffuse reflectance UV/visible absorption spectra (DRUVS) were recorded using a spectrophotometer (Shimadzu UV-2401PC) with an integrating sphere attachment and $BaSO_4$ was used as the reference. The surface atomic composition of C-TiO_2 was determined by X-ray photoelectron spectroscopy (XPS) (Kratos XSAM 800pci) using the Mg Kα line (1253.6 eV) as the excitation source. The binding energies of all peaks were referenced against the Au 4f line originating from the gold powder mixed with C-TiO_2. Gold powder (Aldrich) was dispersed on the surface of C-TiO_2 pellet and pressed. The XPS analysis was carried out without Ar^+ ion sputtering for cleaning the sample because the energetic ion bombardment may disrupt the carbon dopants in the lattice.

The time-resolved diffuse reflectance spectroscopy (TDRS) measurements were performed using the second or third harmonic generation (532 and 355 nm, 5 ns full-width at half-maximum) from a Q-switched Nd^{3+}:YAG laser (Continuum, Surelite II-10) for the excitation operated with temporal control by a delay generator (Stanford Research System, DG535). The experimental details are found elsewhere [10].

2.2. Photocatalytic activity test

The photocatalyst powder was suspended in distilled water (1 g/L) under simultaneous ultra-sonication and shaking for 30 s in an ultrasonic cleaning bath. An aliquot of the substrate stock solution was subsequently added to the suspension to give a desired substrate concentration, and then the pH of the suspension was adjusted with $HClO_4$ or NaOH standard solution. Photo-irradiation employed a 300-W Xe arc lamp (Oriel) as a light source. Light passed through a 10-cm IR water filter and a UV cutoff filter ($\lambda > 420$ nm) for visible light irradiation, then the filtered light was focused onto a 30-mL Pyrex reactor with a quartz window. When the wavelength-dependency was tested, different UV cutoff filters were used. The incident light intensity of UV ($300\ nm < \lambda < 500\ nm$) and visible light ($420\ nm < \lambda < 500\ nm$) was determined by ferrioxalate actinometry to be 2.3×10^{-3} and 6.7×10^{-4} einstein $L^{-1}\ min^{-1}$, respectively. Sample aliquots were withdrawn from the reactor at a specific time interval during the illumination and filtered through a 0.45-μm PTFE syringe filter (Millipore) to remove the photocatalyst particles. Duplicate or triplicate photocatalytic degradation (PCD) experiments were carried out under each experimental condition to confirm the reproducibility.

The degradation of 4-chlorophenol (4-CP, Sigma) and the production of intermediates were monitored using a high performance liquid chromatography (HPLC, Agilent 1100 series) equipped with a diode array detector and a ZORBAX 300SB C18 column (4.6 mm × 150 mm). The eluent consisted of a binary mixture of water containing 0.1% phosphoric acid and acetonitrile (80:20 by volume). The generation of chloride from 4-CP degradation was quantified by using an ion chromatograph (IC, Dionex DX-120) that was equipped with a Dionex IonPac AS 14 (4 mm × 250 mm) column and a conductivity detector. Dissolved organic carbon was measured using a total organic carbon analyzer (TOC-VCSH, Shimadzu). The photocatalytic oxidation of iodide (I^-) to triiodide (I_3^-) was also carried out as a test reaction. The triiodide production was spectrophotometrically monitored by measuring the absorbance at 352 nm [24].

Measurements of the photocurrent collected on an inert electrode (Pt) immersed in aqueous suspension of TiO_2 or C-TiO_2 were carried out with a potentiostat (EG&G 263A2) [25]. Fe^{3+}/Fe^{2+} redox couple was used as an electron shuttle that carries the electron from the photocatalyst particles to the Pt electrode. Pt plate (1 cm × 1 cm), a saturated calomel electrode (SCE), and a graphite rod were used as a working, a reference and a counter electrode, respectively.

3. Results and discussion

3.1. Evidences of carbon dopants in TiO_2

Fig. 1a shows the XRD patterns of the synthesized TiO_2 powder that was treated at various calcination temperatures. The TiO_2 powder obtained through the sol–gel process had primarily the anatase phase, and the rutile phase appeared when the temperature increased between 300 and 400 °C and grew substantially high at 500 °C. The crystalline particle size and the BET surface area of the TiO_2 sample powders calcined at various temperatures were summarized in Table 1. With increasing the temperature up to 500 °C, the surface area steadily decreased with increasing the particle size.

Fig. 1b displays the diffuse reflectance UV–visible spectra (DRUVS) of the prepared TiO_2 samples and Degussa P25 as a reference material. The bandgap energy (E_g) of each catalyst was determined by extrapolating the linear portion of the absorption edge to the abscissa. The TiO_2 samples prepared at 80 °C (TiO_2@80) and 400 °C (TiO_2@400) have a similar reflectance onset energy (i.e., E_g) of around 3.0–3.1 eV, which is very similar to P25 ($E_g \sim 3.26$ eV) (Table 1). On the other hand, TiO_2@250 exhibits a narrower bandgap of 2.8 eV and its visible light absorption tailed down to 1.5 eV. Although TiO_2@300 and TiO_2@400 were similar in the onset energy, TiO_2@300 has a markedly higher visible absorption tailing down to 2.3 eV. The visible colour of the catalyst powder was changed with varying the calcination temperature. The catalyst samples calcined between 250 and 400 °C were coloured (yellowish to brown) but became white below or above the temperature range (Table 1). The lower E_g of TiO_2@500 could be attributed to the appearance of rutile phase which has a smaller bandgap than anatase by ca. 0.2 eV.

The calcination temperature-dependent property change of the prepared TiO_2 was investigated by XPS analysis. Fig. 2a compares the XPS profiles in the region of C 1s binding energy (BE) among the TiO_2 samples prepared with varying the calcination temperature. Primary C 1s-relevant peaks were found mainly at three BEs: 285.5, 287 and 288.7 eV (Fig. 2b). Fig. 2b shows the deconvoluted components (peaks 1–3) for the carbon band of TiO_2@250. The BE at 285.5 eV (peak 1) that is also observed with the reference P25

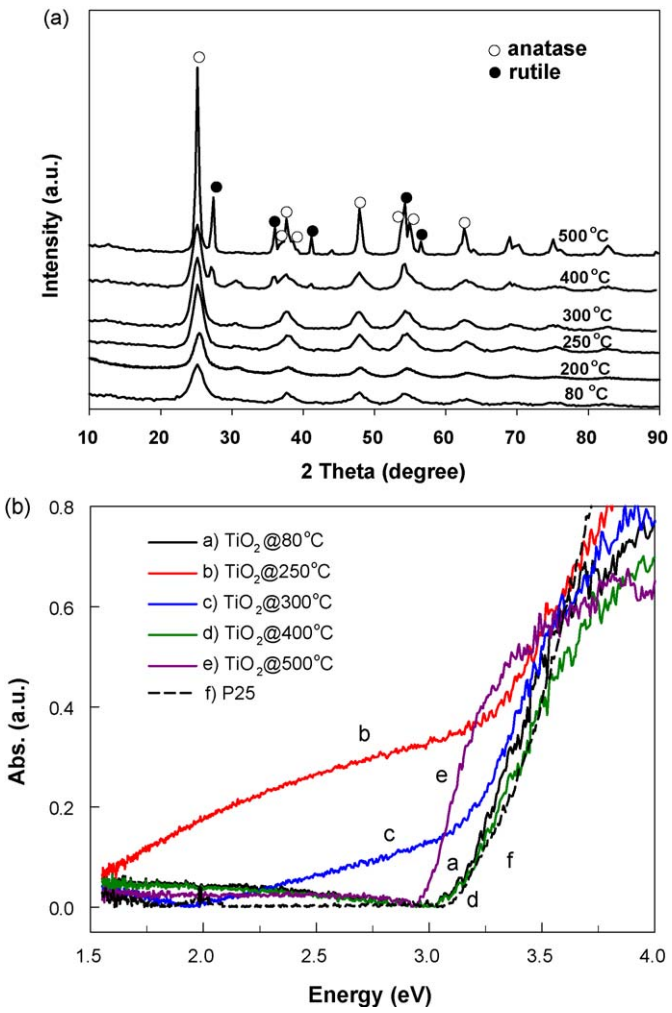

Fig. 1. (a) X-ray diffraction (XRD) patterns of TiO_2 samples treated at various calcination temperatures. (b) Diffuse reflectance UV–visible spectra of TiO_2 samples (a–e, 80–500 °C) treated at various calcination temperatures. Pure TiO_2 (P25), f, is compared as a reference material.

should be ascribed to ambient organic impurities adsorbed on the surface of TiO_2. This band (peak 1) gives little information about the carbon dopants. The BE peaks centered at 287 eV (peak 2) and 288.7 eV (peak 3) are similar to those of oxidized carbon species such as C-OR(H), C=O, C–OOR(H) that may be associated with the carbon residues on the surface of TiO_2. However, a more plausible assignment in this case should be related with the carbonate species as an interstitial dopant [15–18,26,27]. The intensities of peak 2 and 3 markedly increased from TiO_2@80 to TiO_2@200 and then gradually decreased with increasing the calcination temperature from 200 to 500 °C. The carbon band of TiO_2@500 was qualitatively similar to that of TiO_2@80, which implies that the carbon doping is not favoured at higher temperature. The anionic carbon species (a substitutional dopant with Ti–C bond) that should be found around 282 eV was not observed at all.

Table 1
Physical properties of TiO_2 powder calcined at various temperatures.

Catalyst (Temp.)	Particle size (nm)[a]	E_g (eV)	BET surface area (m^2/g)	Catalyst color
80 °C	(A) 5.7	3.15	258	White
250 °C	(A) 4.9	2.8	195	Brown
300 °C	(A) 16.6	3.04	172	Brown
400 °C	(A) 41.8, (R) 16.6	3.12	123	Pale yellow
500 °C	(A) 16.6, (R) 27.8	2.98	46	White
P25[b]	(A) 26.2, (R) 32.7	3.26	53	White

[a] Determined from the XRD pattern using the Sherrer formula.
[b] Reference commercial TiO_2 sample for comparison.

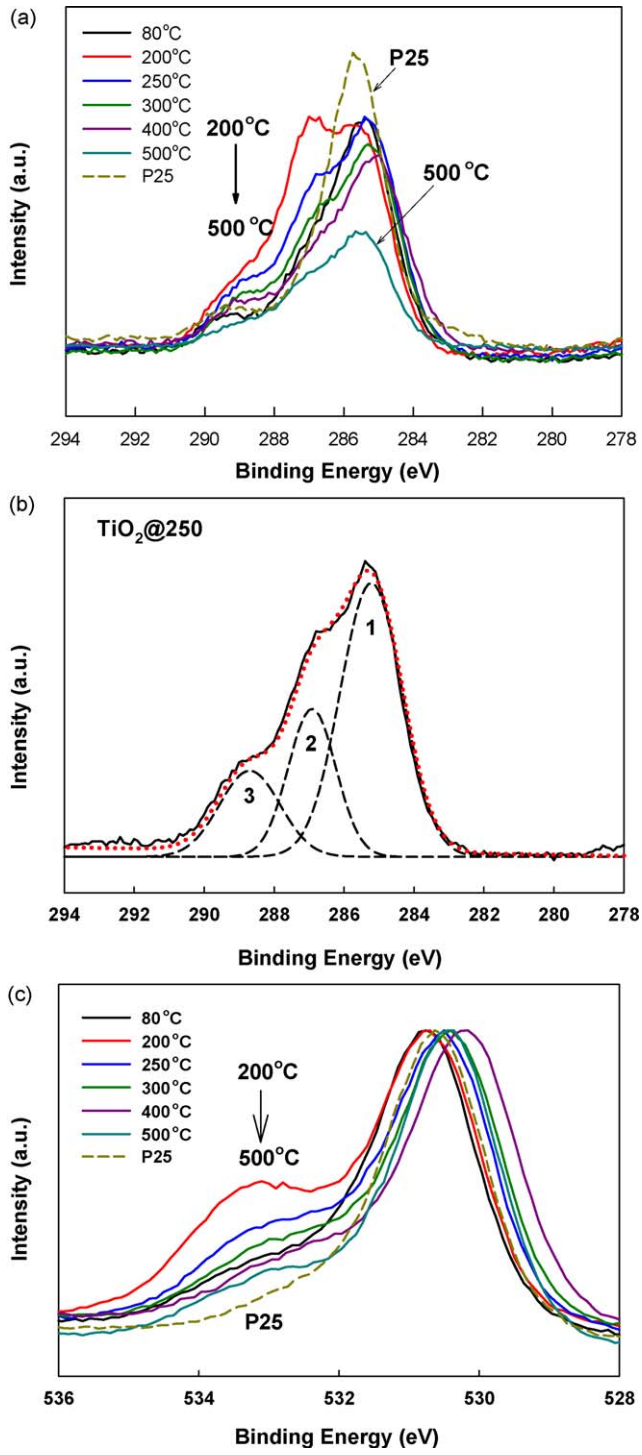

Fig. 2. (a) The XPS spectra of the C 1s band for TiO_2 samples treated at various calcination temperatures. (b) Deconvolution of the C 1s band of TiO_2@250 into three components [1: 285.2 eV, 2: 287 eV, and 3: 288.7 eV], the dotted-line is the sum of the three fitting components. (c) The XPS spectra of the O 1s band for TiO_2 samples treated at various temperatures (spectra were normalized at the peak intensity).

The incorporation of carbon into the oxide lattice should influence the BE of O 1s as well. Fig. 2c shows that TiO_2 samples calcined between 80 and 400 °C have two main peaks: one at around 530–531 eV for the regular lattice oxygen and the other at 533 eV which is ascribed to the oxygen in the carbonate [27]. The

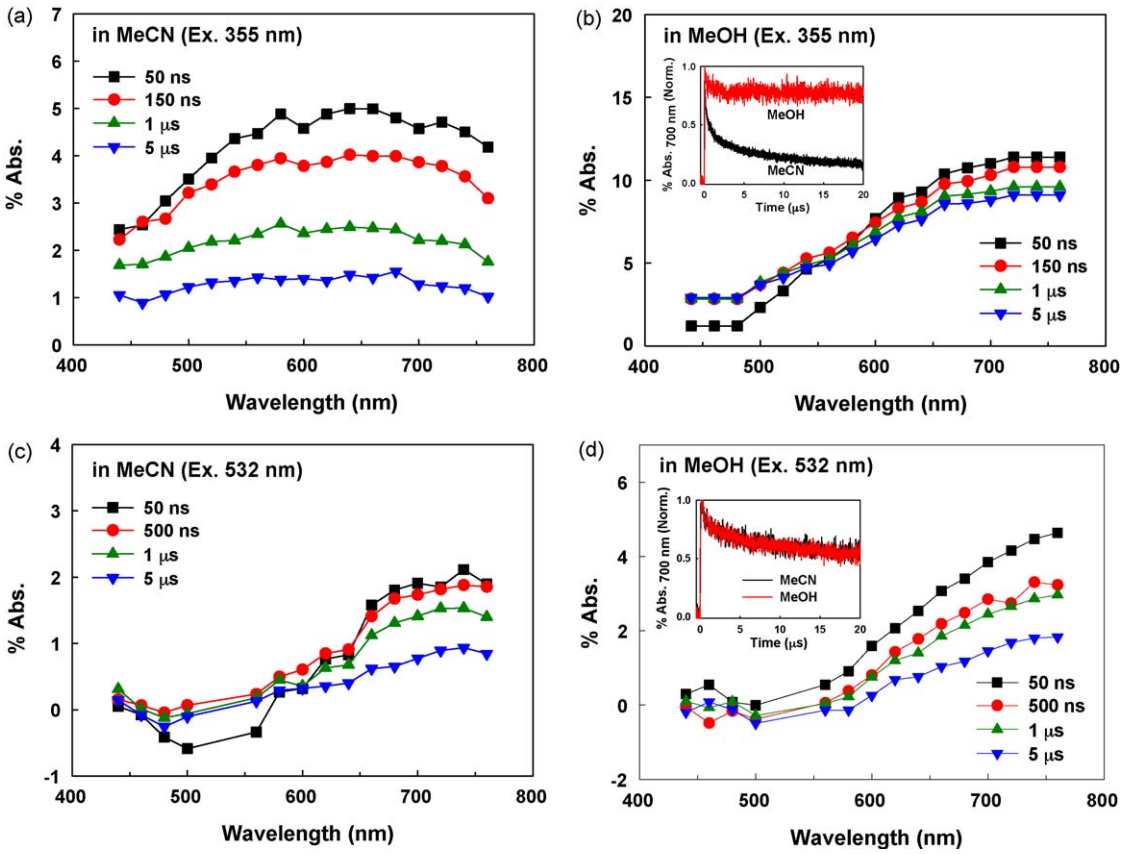

Fig. 3. TDR spectra observed at 0.05, 0.15, 0.5, 1, and 5 μs after the laser flash during the 355-nm (a and b) and 532-nm (c and d) laser photolysis of the TiO_2@250 in O_2-saturated CH_3CN (a and c) and CH_3OH (b and d), respectively. Inset: time traces observed at 700 nm during the 355-nm (or 532-nm) laser flash photolysis of the TiO_2 @250 in O_2-saturated CH_3CN (red line) and CH_3OH (black line). (For interpretation of the references to color in this figure legend, the reader is referred to the web version of the article.)

BE of the former peak drifts by ~0.6 eV depending on the calcination temperature (lowering BE from 200 to 400 °C), which might be related with the creation of oxygen vacancies as a result of the carbon doping. The latter peak is maximal around 200 °C and gradually reduced with increasing the calcination temperature up to 500 °C. This observation is consistent with the fact that the intensities of the carbon dopant peaks were gradually reduced with increasing the calcination temperature from 200 to 500 °C (see Fig. 2a). The BE shift in both C 1s and O 1s region indicates that carbons can be indeed incorporated into the lattice at lower calcination temperatures even in the absence of external carbon precursors. The carbon source should be the titanium alkoxide precursor itself. The incorporation of carbon dopants was hindered with increasing the calcination temperature and TiO_2@500 seems to be largely free from carbon dopants. Incidentally, a similar sol–gel preparation of TiO_2 using titanium isopropoxide or ethoxide as a precursor was also tried but not as efficient as the butoxide precursor for carbon doping, which implies that the kind of alkoxide precursor sensitively influences the incorporation of the carbon dopants into the lattice.

3.2. Transient charge carrier dynamics in C-TiO_2

To explore the characteristics of the impurity-induced energy levels and the behaviours of the photogenerated charge carriers in the prepared TiO_2@250, the time-resolved diffuse reflectance spectroscopy (TDRS) study was performed with employing two excitation wavelengths: 355 nm for UV and 532 nm for visible light. The TDR spectra with the 355 nm-excitation were obtained in both acetonitrile (MeCN) (Fig. 3a) and methanol (MeOH) (Fig. 3b) under the O_2-saturated condition. MeCN has low reactivity with holes whereas MeOH is an efficient hole scavenger (for comparison, $k_{OH+MeCN} = 2.2 \times 10^7\ M^{-1}\ s^{-1}$; $k_{OH+MeOH} = 9.7 \times 10^8\ M^{-1}\ s^{-1}$) [28]. It is noted that the transient absorbances were generally smaller in MeCN than MeOH. The charge recombination occurs rapidly within a laser flash (5 ns) in MeCN to show the smaller absorbance of the trapped hole and electron, while the hole is scavenged by MeOH to show the larger absorbance of the trapped electron. The spectral shape obtained in MeCN is also different from that in MeOH. A broad absorption band ranging from 440 to 750 nm in MeCN (Fig. 3a) is attributed to the combination of trapped holes (h_{tr}^+ with 440–650 nm absorption) [10,29] and trapped electrons (e_{tr}^- with 440–760 nm absorption) [10,29] whereas the preferential absorption around 650–750 nm in MeOH (Fig. 3b) indicates the dominance of trapped electrons (e_{tr}^-). As compared in Fig. 3b inset, the time profiles observed at 700 nm (during the 355-nm-laser flash photolysis) are quite different between two solvents. The transient absorbance in MeCN is quickly quenched within 5 μs whereas that in MeOH is maintained up to 20 μs and beyond. This supports that the holes generated in TiO_2@250 are efficiently scavenged by MeOH with retarding the recombination. On the other hand, in the case of the 532-nm-laser photolysis where the intrinsic bandgap transition cannot occur, the TDR spectra and their time profiles are very similar between MeCN and MeOH (Fig. 3c and d). The generation of the transient absorption by the sub-bandgap (visible light) excitation confirms the presence of the impurity dopants in the bandgap. Both spectra show that the absorption of h_{tr}^+ is very weak or absent. This spectral feature (little sign of absorption of h_{tr}^+) may be complicated by the possible bleaching (during laser photolysis)

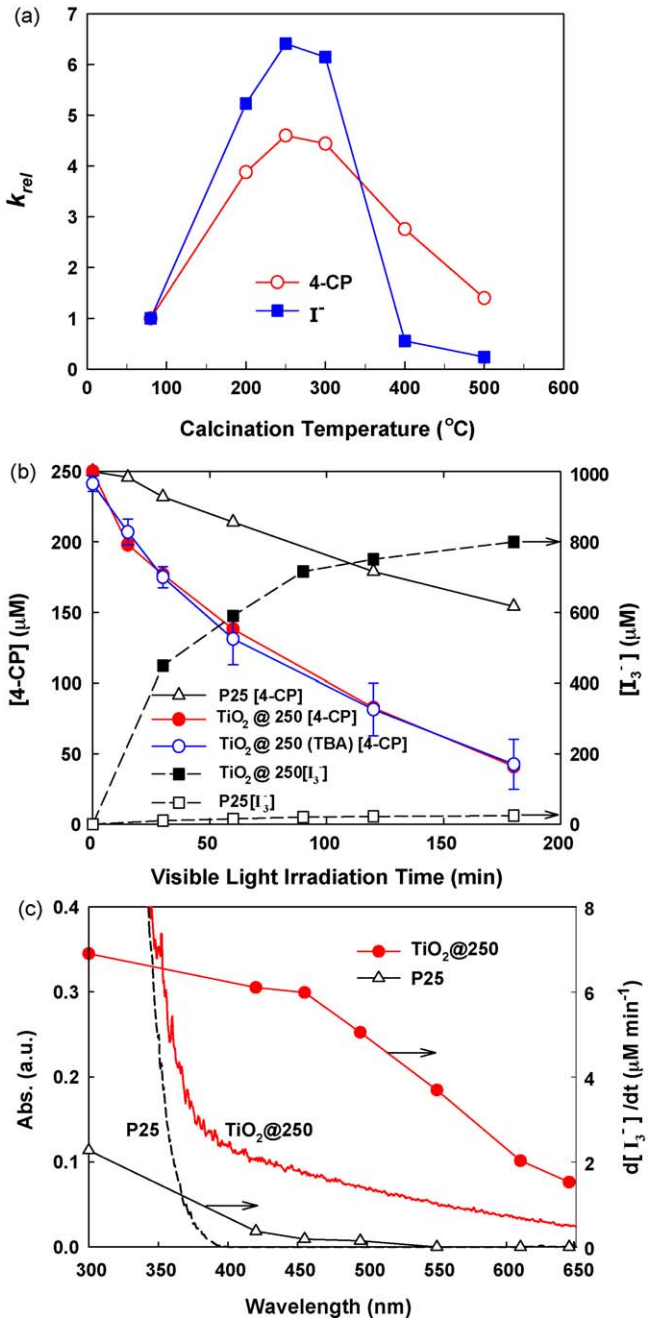

Fig. 4. (a) The variation of the relative reaction rates (k_{rel}) for 4-CP and iodide conversion among various TiO_2@Temp samples. k_{rel} was referenced against the activity of TiO_2@80 under visible light irradiation for 3 h. (b) Time profiles of the photocatalytic degradation of 4-CP and oxidation of iodide in the visible light-irradiated suspensions of the reference TiO_2 (P25) and TiO_2@250. (c) The photocatalytic oxidation rates of I^- with P25 and TiO_2@250 as a function of the irradiation wavelength compared along with their diffuse reflectance UV–visible spectra. The wavelength in the abscissa refers to the cutoff λ (where $I_t/I_0 = 0.5$) of the long-pass filter (λ_{irrad} > cutoff λ). *Experimental conditions*: [TiO_2] = 1 g/L; λ > 420 nm (except the case of c); $[4\text{-CP}]_0$ = 0.25 mM; $[I^-]_0$ = 10 mM; pH_i = 3; [TBA] = 100 mM (when indicated).

of the ground-state absorption of C-TiO_2 in the visible region because the visible absorption bands of h_{tr}^+ and C-TiO_2 (see Fig. 1b) overlap. Another possibility is that most holes are trapped at midgap states which have no absorption in the present wavelength region (440–760 nm). It should be noted here that a longer lifetime of the charge carriers was observed for the 532-nm excitation in MeCN (where holes are not scavenged by the solvent molecules), compared with that for the 355-nm excitation. This suggests that the localized states in the resulting band structure of TiO_2 doped with C atoms influence the trapping and detrapping processes of charge carriers. Similar laser photolysis results were also reported for C-TiO_2 that was prepared using an external carbon precursor [10]. Therefore, we assume that the holes generated from the midgap level (h_{mid}^+), which might be created via the hybridization of O 2p and C-derived states, have lower oxidation potential and little reactivity with MeOH. This implies that the present synthesis method using no external carbon precursor produced C-TiO_2, which has similar characteristics to typical C-TiO_2 reported in the literature.

3.3. Photocatalytic activities under visible light

The as-prepared TiO_2 samples were investigated for their photocatalytic activities with two model substrates, 4-CP and iodide (I^-), under visible light (λ > 420 nm) irradiation. Since the level of carbon doping seems to be sensitively dependent on the calcination temperature, the photocatalytic activities of the TiO_2 samples prepared in this work should vary with the calcination temperature. Fig. 4a shows the variation of the visible light photocatalytic activities for 4-CP and iodide conversion among TiO_2 samples calcined at various temperatures. The photocatalytic activities are expressed in terms of the relative reaction rate of 4-CP and iodide (k_{rel}), which is defined as the ratio $k(TiO_2@Temp)/k(TiO_2@80)$. The visible light activities for both substrates show a volcano-shaped behaviour with the maximum around 250 °C. This is consistent with the fact that the visible light absorption and the content of C-dopants (C_{dop}) is maximal with TiO_2@250. Accordingly, the optimal calcination temperature was fixed at 250 °C and TiO_2@250 was used in further experiments.

In Fig. 4b, the time profiles of the photoconversion of 4-CP and iodide under visible light are compared between TiO_2@250 and P25. The reference P25 shows no activity for iodide conversion but a moderate activity for the degradation of 4-CP. The visible light activity of pure TiO_2 for the degradation of 4-CP was demonstrated by this group and is ascribed to the surface-complex mediated charge transfer mechanism [30] which enables the degradation of 4-CP without the involvement of holes. The visible light induced degradation of 4-CP with TiO_2@250 was much enhanced compared with P25. The 4-CP degradation on TiO_2@250 accompanied the production of chlorides and the reduction of total organic carbon (TOC) by 65% (in 3 h). This evidences that 4-CP is mineralized on TiO_2@250 under visible light. While the photocatalytic degradation of organic compounds on UV-irradiated TiO_2 is largely mediated by the generation of OH radicals, the visible light-irradiated TiO_2@250 (i.e., C-TiO_2) may not be energetic enough to generate OH radicals. Fig. 4b shows the addition of *t*-butyl alcohol (TBA: OH radical scavenger) in the visible light-irradiated suspension of TiO_2@250 has no effect on the degradation of 4-CP. On the other hand, the addition of TBA significantly reduces the removal rate of 4-CP in UV-irradiated suspension of pure TiO_2 [30]. This supports that OH radicals are not generated on the visible light-irradiated TiO_2@250. The major oxidants in TiO_2@250 photocatalysis should be holes trapped in the midgap states (h_{mid}^+) and their oxidation potential seems to be strong enough to directly oxidize 4-CP ($E(4\text{-CP}^{\bullet+}/4\text{-CP}) = 0.8$ V vs NHE) [31] but not enough to generate OH radical ($E(HO^\bullet/HO^-) = 1.9$ V vs NHE) [32].

As for the photocatalytic oxidation of iodide, the reaction of h_{mid}^+ with I^- leads to the generation of iodine (I_2) or triiodide ($I_3^{\bullet-}$) through the following steps (Eqs. (1)–(4)) [24]:

$$h_{mid}^+ + I^- \rightarrow I^\bullet \quad (1)$$

$$I^\bullet + I^- \leftrightarrow I_2^{\bullet-} \quad (2)$$

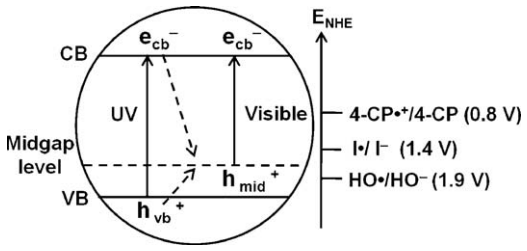

Scheme 1. Schematic illustration of the photocatalysis occurring on the as-prepared C-TiO_2 under UV or visible light irradiation. CB and VB denote the conduction and valence band of the TiO_2 particle, respectively. The broken line represents the C-induced midgap level that should lie between 1.4 and 1.9 V_{NHE}.

$$I_2^- + I_2^- \rightarrow I_3^- + I^- \quad (3)$$

$$I_3^- + e_{cb}^- \rightarrow I_2^- + I^- \quad (4)$$

where $k_2 > 1.2 \times 10^4$ and $k_3 = 3.2 \times 10^9\ M^{-1}\ s^{-1}$[33]. Since holes cannot be generated on the visible light-irradiated TiO_2, the oxidation of iodide is negligible with P25 as shown in Fig. 4b. The production of triiodide with TiO_2@250 is outstanding and is leveled off in 2 h probably due to reaction (4). The carbon doping is supposed to create several localized midgap/surface states above the TiO_2 valence band rendering visible light absorption [9]. Considering that the reduction potential of ($I^{\bullet}/I^-$) couple is 1.27–1.42 V_{NHE} [32], the energy level of h_{mid}^+ in TiO_2@250 synthesized in this work should lie between 1.4 and 1.9 V_{NHE} ($E(HO^{\bullet}/HO^-)$). The proposed energy levels in the present C-TiO_2 is illustrated in Scheme 1. The photocatalytic activities of TiO_2@250 for the iodide oxidation were measured as a function of the irradiation wavelength. Fig. 4c compares the activities (for iodide conversion) between P25 and TiO_2@250 along with their DRUV spectra. The visible light activity of TiO_2@250 is extended up to 650 nm whereas that of P25 is negligibly small above 420 nm. Such wavelength dependences are qualitatively consistent with the optical absorption profiles of P25 and TiO_2@250.

The above photocatalytic reactions of 4-CP and iodide that mainly involve the hole transfer should be accompanied by the concurrent electron transfer on C-TiO_2. To investigate the photogenerated electron transfer process, the photocurrent was collected from the suspension of C-TiO_2 (TiO_2@250) under visible light irradiation. We employed an electrochemical method that utilizes the redox couple of (Fe^{3+}/Fe^{2+}) as an electron shuttle and EDTA as a hole scavenger [25]:

$$\text{C-}TiO_2 + h\nu \rightarrow h_{mid}^+ + e_{cb}^- \quad (5)$$

$$e_{cb}^- + Fe^{3+} \rightarrow Fe^{2+} \quad (6)$$

$$h_{mid}^+ + EDTA \rightarrow EDTA^+ \quad (7)$$

$$Fe^{2+} + Pt(\text{electrode}) \rightarrow Fe^{3+} + Pt(e^-) \quad (8)$$

Fig. 5 compares the time profiles of the photocurrent generation in the suspensions of P25 and TiO_2@250. The much higher level of photocurrent obtained with TiO_2@250 is consistent with the photocatalytic activity data and reassures that TiO_2@250 is active under visible light. The fact that the non-negligible photocurrent was generated in the visible light-irradiated suspension of P25 might be ascribed to ligand-to-metal charge transfer in the EDTA–TiO_2 surface complex. This phenomenon is currently being investigated in detail.

The origin of the photocatalytic activity of the C-TiO_2 under visible light irradiation is mostly ascribed to the presence of C_{dop} in the lattice of TiO_2 but other factors may contribute. The surface carbon species on TiO_2 (e.g., coke-containing TiO_2) [34] may work

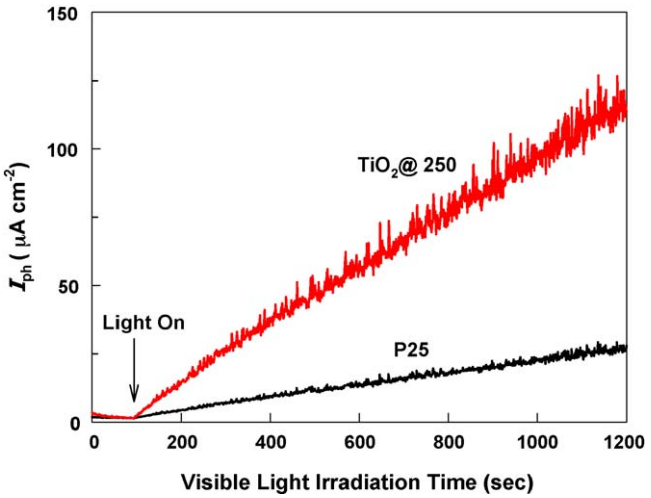

Fig. 5. The comparison of Fe^{3+}-mediated photocurrent collected on a Pt electrode in the deaerated suspension of TiO_2@250 and pure TiO_2 (P25). *Experimental conditions*: $[Fe^{3+}] = 0.1$ mM; $[LiClO_4] = 0.1$ M; $[EDTA]_0 = 10$ mM; $pH_i = 1.6$.

as a photosensitizer. The surface carbon species present on TiO_2 is expected to be oxidized into CO_2 through photocatalysis under UV irradiation. To assess the effect of the surface carbon species on the visible light photocatalytic activity, TiO_2@250 was pre-irradiated under UV light ($\lambda > 300$ nm) prior to carrying out the visible light photocatalysis reactions. Since the UV photocatalysis should remove the surface impurity carbon species, the carbon-sensitized activity, if any, should be reduced after the pre-irradiation. Fig. 6a compares the visible light activity for 4-CP degradation in terms of %degradation, $(C_0 - C_{3h})/C_0 \times 100\%$, as a function of the UV pre-irradiation time. The pre-irradiation of 1 h slightly decreased the visible light activity of TiO_2@250 but further UV irradiation did not decrease the activity any more. This indicates that most surface carbon species on TiO_2@250 that may act as a sensitizer was removed photocatalytically during 1 h of pre-irradiation and that the remaining visible light activity of TiO_2@250 is largely ascribed to the presence of C_{dop}. The visible light activity of TiO_2@250 was maintained through the repeated uses of the same batch of the catalyst with no significant deactivation (Fig. 6b). This indicates that the C_{dop} in TiO_2@250 is quite stable during the irradiation.

4. Conclusions

This study demonstrates that the carbon-doped TiO_2 could be successfully obtained from a sol–gel synthesis process even without using external carbon precursors such as urea and alkylammonium that have been frequently employed. The carbons contained in titanium alkoxide precursor can be incorporated into the lattice of TiO_2 through the controlled calcination. It should be emphasized that the visible light activity induced by the carbon doping closely depends on how it is prepared. The visible light activity that was quantified in terms of the conversion rate of 4-CP and iodide was sensitively influenced by the calcination temperature with showing the best activity around 250 °C. Increasing the calcination temperature above 300 °C rapidly removed the visible light activity, indicating that the incorporation of the lattice carbons is hindered at higher temperatures. The XPS analysis showed that carbon dopants were mainly carbonate species and no carbide species were present. Various characterizations including optical absorption, TDRS, photocurrent, and photocatalytic activity measurements support that the incorporation of carbon dopants created midgap energy levels in TiO_2 with inducing the visible light activity. The findings from this study imply that C-TiO_2 might be

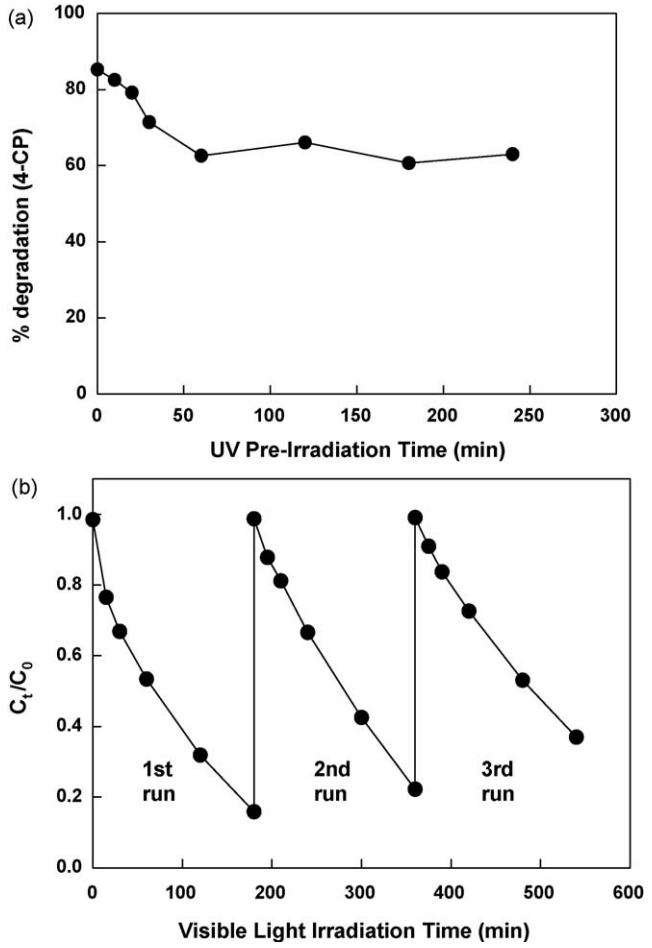

Fig. 6. (a) Effects of UV pre-irradiation ($\lambda > 300$ nm) time on the degradation ($((C_0 - C_{3h})/C_0 \times 100\%$) of 4-CP in the visible light-irradiated suspension of TiO_2@250. (b) The multi-cycles of 4-CP degradation with the same batch of TiO_2@250 under visible light. [TiO_2] = 1 g/L; $\lambda > 420$ nm; $[4\text{-CP}]_0$ = 0.25 mM.

unintentionally obtained through the conventional sol–gel synthesis that uses titanium alkoxide precursors. The preparation conditions such as the calcination temperature and the kind of the carbon precursor sensitively influences the incorporation of carbon dopants and their chemical states, which needs to be further investigated for better understanding.

Acknowledgements

This work was supported by a KOSEF grant (No. R0A-2008-000-20068-0), the KOSEF EPB center (Grant No. R11-2008-052-02002), and BK 21 program. T.M. and T.T. thank to a Grant-in-Aid for Scientific Research (Project 17105005, 19750115) from MEXT (Japan).

References

[1] M.R. Hoffmann, S.T. Martin, W. Choi, D.W. Bahnemann, Chem. Rev. 95 (1995) 69–96.
[2] D. Duonghong, E. Borgarello, M. Gratzel, J. Am. Chem. Soc. 103 (1981) 4685.
[3] E. Bae, W. Choi, J. Park, H.S. Shin, S.B. Kim, J.S. Lee, J. Phys. Chem. B 108 (2004) 14093.
[4] H. Kisch, L. Zang, C. Lange, W.F. Maier, C. Antonius, D. Meissner, Angew. Chem., Int. Ed. 37 (1998) 3034.
[5] C. Wang, D.W. Bahnemann, J.K. Dohrmann, Chem. Commun. 16 (2000) 1539.
[6] H. Yamashita, M. Honda, M. Harada, Y. Ichihashi, M. Anpo, T. Hirao, N. Itoh, N. Iwamoto, J. Phys. Chem. B 102 (1998) 10707.
[7] R. Asahi, T. Morikawa, T. Ohwaki, K. Aoki, Y. Taga, Science 293 (2001) 269–271.
[8] S. Livraghi, M.C. Paganini, E. Giamello, A. Selloni, C.D. Valentin, G. Pacchioni, J. Am. Chem. Soc. 128 (2006) 15666–15671.
[9] C.D. Valentin, G. Pacchioni, A. Selloni, Chem. Mater. 17 (2005) 6656–6665.
[10] T. Tachikawa, S. Tojo, K. Kawai, M. Endo, M. Fujitsuka, T. Ohno, K. Nishijima, Z. Miyamoto, T. Majima, J. Phys. Chem. B 108 (2004) 19229–19306.
[11] S.U.M. Khan, M. Al-Shahry, W.B. Ingler Jr., Science 297 (2002) 2243–2244.
[12] Y. Choi, T. Umebayashi, M. Yoshikawa, J. Mater. Sci. 39 (2004) 1837–1839.
[13] H. Irie, Y. Watanabe, K. Hashimoto, Chem. Lett. 32 (2003) 772–773.
[14] S.-W. Hsu, T.-S. Yang, T.-K. Chen, M.-S. Wong, Thin Solid Films 515 (2007) 3521–3526.
[15] Y. Li, D.-S. Hwang, N.H. Lee, S.-J. Kim, Chem. Phys. Lett. 404 (2005) 25–29.
[16] T. Ohno, T. Tsubota, K. Nishijima, Z. Miyamoto, Chem. Lett. 33 (2004) 750–751.
[17] W. Ren, Z. Ai, F. Jia, L. Zhang, X. Fan, Z. Zou, Appl. Catal. B: Environ. 69 (2007) 138–144.
[18] S. Sakthivel, H. Kisch, Angew. Chem. Int. Ed. 42 (2003) 4908–4911.
[19] T. Torimoto, Y. Okawa, N. Takeda, H. Yoneyama, J. Photochem. Photobiol. A: Chem. 103 (1997) 153–157.
[20] B. Tryba, A.W. Morawski, M. Inagaki, Appl. Catal. B 41 (2003) 427–433.
[21] B. Tryba, T. Tsumura, M. Janus, A.W. Morawski, M. Inagaki, Appl. Catal. B: Environ. 50 (2004) 177–183.
[22] T. Tsumura, N. Kojitani, M. Toyoda, M. Inagaki, J. Mater. Chem. 12 (2002) 1391–1396.
[23] D.-E. Gu, Y. Lu, B.-C. Yang, Y.-D. Hu, Chem. Commun. (2008) 2453–2455.
[24] C. Kormann, D.W. Bahnemann, M.R. Hoffmann, J. Phys. Chem. 92 (1988) 5196–5201.
[25] H. Park, W. Choi, J. Phys. Chem. B 180 (2004) 4086.
[26] E. Papirer, r. Lacroix, J.-B. Donnet, G. Nanse, P. Fioux, Carbon 33 (1995) 63–72.
[27] R. Fu, N. Yoshizawa, M.S. Dresselhaus, G. Dresselhaus, J.H. Satcher Jr., T.F. Baumann, Langmuir 18 (2002) 10100–10104.
[28] G.V. Buxton, C.L. Greenstock, W.P. Helman, A.B. Ross, J. Phys. Chem. Ref. Data 17 (1998) 513–886.
[29] D. Bahnemann, A. Henglein, J. Lilie, L. Spanhel, J. Phys. Chem. 88 (1984) 709–711.
[30] S. Kim, W. Choi, J. Phys. Chem. B 109 (2005) 5143–5149.
[31] U. Stafford, K.A. Gray, P.V. Kamat, J. Phys. Chem. 98 (1994) 6343.
[32] P. Wardman, J. Phys. Chem. Ref. Data 18 (1989) 1637–1755.
[33] L.M. Dane, L.J.J. Janssen, J.G. Hoogland, Electrochim. Acta 13 (1968) 507–518.
[34] C. Lettmann, K. Hildenbrand, H. Kisch, W. Macyk, W.F. Maier, Appl. Catal. B: Environ. 32 (2001) 215–227.